Geotextiles and Geomembranes 45 (2017) 149–160

Contents lists available at ScienceDirect

Geotextiles and Geomembranes

journal homepage: www.elsevier.com/locate/geotexmem

Shock wave attenuation by geotextile encapsulated sand barrier systems

Padmanabha Vivek*, Thallak G. Sitharam

Department of Civil Engineering, Indian Institute of Science, Bangalore 560012, India

ARTICLE INFO

Article history:
Received 29 March 2016
Received in revised form
2 December 2016
Accepted 3 January 2017
Available online 15 February 2017

Keywords:
Geosynthetics
Shock waves
Attenuation
Sand

ABSTRACT

This paper presents a laboratory scale experimental technique to study the performance of the encapsulated sand barrier systems in mitigating shock waves. The geotextile encapsulated sand barrier systems are made of cubical wire mesh formwork lined with geotextile and form a thick protective barrier when filled with granular materials. In the present study, dry sand particles of size varying from microns to few millimeters (fine and coarse) are used as infill granular material. Spherical shaped glass beads are also used as the infill material to study the influence of shape of the infill particle on the attenuation behavior. The process of shock wave attenuation by the sand barrier, with and without the geotextile facing formwork is examined. The experiments are performed using a conventional shock tube, where shock waves with incident Mach number in the range of 1.29–1.70 are generated. The experimental results show that the presence of geotextile layer has contributed significantly towards shock wave attenuation. The geotextile also plays an important role as a regulator, which is able to deliver gradual pressure rise at the downstream end of the barrier.

1. Introduction

Upon explosion, a high intensity shock wave front arises, causing physical damage to structures and destruction of lives. Structural steel and reinforced concrete structures are commonly used as protective structures against explosion. Although these structures have high tolerance in mitigating the blast, upon extreme blast loads, the structures collapse leading to generation of debris particles and sharp fragments. Most of the concrete and steel structures are permanent and involve considerable time and labour for the construction. Alternately, sand bags are commonly used as protective barrier walls. The function of the temporary wall is to shield against the blast/shock effect from various sources like terrorist attacks, battle field and accidental detonation of stored explosives, munitions etc.

Geotextile contained sand barriers are prefabricated type of protective structures which are cost effective, easy to setup and easily mobilizable to different site conditions. Moreover, these barriers do not undergo brittle failure like concrete walls upon blast impact (Ng et al., 2000). One such commercially available product which has found extensive use in military application is HESCO Bastion Concertainer wall barriers (Scherbatiuk and Rattanawangcharoen, 2008). The concertainer barriers are cubical baskets made of stainless steel wire mesh lined with nonwoven geotextile and they form a protective barrier system upon filling with locally available granular material like sand and gravels (see Fig. 1a–b). The granular barrier system also finds use in various industrial and commercial applications. For instance, they are used as ventilation seals in the mining industry (Fig. 1c) to protect the mine workers from the violent explosions and prevent the outburst gases entering the confined working chambers (Sapko et al., 2009).

Geotextiles are widely used in geotechnical engineering as a separation and reinforcement medium (Ling et al., 2003; Koerner and Soong, 2001). Under purview of geotextile-granular interaction, researchers have extensively studied the effects of particle shape and size (Athanasopoulos, 1993; Afzali-Nejad et al., in press), interlocking behavior between geotextile and sand particles (Lee and Manjunath, 2000) and interfacial frictional characteristics of sand and the reinforcing materials like geotextile and wire mesh (Vangla and Latha, 2016). In addition, research has been conducted by various researchers to assess geotextile as a protective reinforcement medium (e.g., Koerner et al., 1996; Narejo et al., 1996; Tognon et al., 2000; Bathurst et al., 2006; Wu and Hong, 2009; Portelinha et al., 2014; Guler and Selek, 2014; Liu et al., 2014;

* Corresponding author.
E-mail address: vivek2387@gmail.com (P. Vivek).

http://dx.doi.org/10.1016/j.geotexmem.2017.01.006
0266-1144/

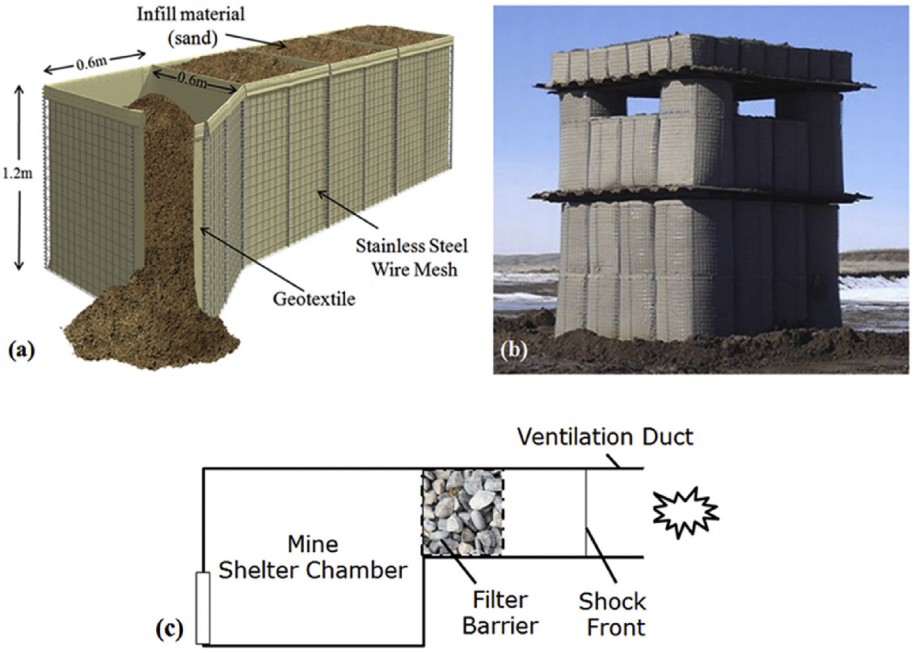

Fig. 1. a–c. (a) An illustrative figure of HESCO Bastion concertainer wall (0.6 × 0.6 × 1.2 m) (b) HESCO bastion units used as a bunker in war field (HESCO, 2010) and (c) Granular particles used as ventilation seals in ducts of mining chambers.

Palmeira and Tatto, 2015; Costa et al., 2016; Hong et al., 2016; Jiang et al., 2016). Most of these experiments were performed under quasi static loading or cyclic loading conditions. Some references on the geotextile used as protective wall are available (Yogendrakumar and Bathurst, 1992; Pieri, 1998; Rose et al., 1998; Smith, 2010). However, the role of geotextile as a blast mitigating medium is not much explored. Among the few available literature, Scherbatiuk and Rattanawangcharoen (2008) have performed full scale field blast test on free-standing, soil-filled, geotextile-lined HESCO concertainer walls and reported displacement-time histories on the wall for different blast pressures. Ng et al. (2000) have carried out several detonation experiments on geosynthetic reinforced soil wall and reinforced earth wall with precast concrete facings and compared the damage patterns between them. Further, Zhiwei (2009) has performed full scale field blast test on geosynthetic faced reinforced soil wall using 5 tons and 27 tons of TNT. Blast induced soil displacements and the overall performance of a reinforced soil wall was studied extensively using strain and pressure measurements on the walls, which are placed at different stand-off distances (30 m, 60 m and 90 m) from the source of the blast. Although, the full scale field blast testing using explosives closely relate to the real site blast conditions, there are some limitations: i) Field blast experiments are very expensive and are highly vulnerable to accidents, ii) Instrumentation and measurements involve a tedious process and in many cases the sensors are damaged and iii) Repeatability is difficult to achieve.

Numerous literature are available on the shock/blast wave attenuation through granular medium alone (Van-der Grinten et al., 1985; Engebretsen et al., 1996; Ben-Dor et al., 1997; Britan et al., 1997, 2001, 2007; Lv et al., in press). Shock tube has been extensively used in the laboratory experiments. Researchers have used various type of granular medium as an obstacle to mitigate the incoming shock wave. Engebretsen et al. (1996) have considered plastic and glass spheres as granular particles and studied the effect of the material density and particle size on the attenuation phenomenon. A series of shock tube experiments were carried out by Ben-Dor et al. (1997) on various types of granular materials (potash, polysterene, nylon, sand etc.) by measuring the pressure in front and inside the granular layers. It was observed that the impact of shock wave has generated a transmitted wave in the granular media (resulting in the compaction of the granular particles) which is governed by gas filtration. Britan et al. (2001) have used ceramic granules of $ZrSiO_4$, steel balls and glass beads as a barrier medium for shock wave attenuation; the transmitted shock through the granular medium was analyzed with respect to the length of the sample and the air gap between the protective structure and the granular sample. In similar experiments, Britan et al. (2007) and Van-der Grinten et al. (1985) have performed shock tube experiments by using long granular sample of length 2.5 m and 1.85 m respectively. Researchers have also investigated the impact of shock wave on various kinds of textile and fabrics. Heffernan et al. (2006) have considered lightweight textile membranes like tarpaulins, synthetic fiber etc. in mitigating the blast wave. They have also proved that woven textile provide better resistance to blast wave when compared to nonwoven textile. The reflection and propagation of shock wave in textile like satin, muslin and polycotton were experimentally investigated by Hattingh and Skews (2001). Instead of the expected attenuation, pressure amplification was observed at region adjacent to the textile layer. The authors have justified the amplification with the two involved mechanisms: i) the transmitted shock wave reflecting back and forth between the end wall and the textile ii) generation of compression waves due to the piston like movement of the textile (Hattingh and Skews, 2001; Skews et al., 2010).

From the above cited literature, it is obvious that granular particles are widely used as attenuating medium for shock waves. Also, most of the previous studies seem to focus on using uniformly shaped smaller size particles having diameters in the range of 0.5 mm–2 mm. The present study considers non-uniform mixtures of local sand with the particle size ranging from 4.75 mm to as small as 75 μm. An encapsulated sand barrier model is developed by using wire mesh and geotextile, as the facing formwork for the infill sand particles. The barrier models are tested in the laboratory using a shock tube. Shock tube is a device used to generate shock

waves and it is known for its apparent simplicity, good repeatability and better experimental control with safe working conditions. The objective of the present work is to illustrate the capability of the sand particles in attenuating the shock wave and assess the role of geotextile as a facing formwork. The paper also examines the stability of the facing formwork (wire mesh and geotextile) on the barrier system through the acceleration response incurred during shock impact loading.

2. Experimental setup

2.1. Shock tube

The shock waves are produced by sudden release of energy during a short period of time. One of the efficient ways to generate shock wave and blast wave in the laboratory is by using shock tube. The shock tube is a long cylindrical tube made of two sections: High pressure chamber (HPC) and Low pressure chamber (LPC), which are separated by a metal diaphragm. High pressure compressed gas (nitrogen or helium) is injected into the HPC, while maintaining the LPC at lower pressure conditions (generally kept at atmospheric pressure). The pressure of the HPC is increased until the diaphragm ruptures and thereby generating a shock wave in the LPC. A typical shock wave profile is characterized by the presence of sharp jump, followed by a plateau (or flattop) region. The sharp jump represents the shock front and the constant plateau is associated with the overpressure (pressure caused by a shock wave over and above the atmospheric pressure) region of the incident shock wave. A blast wave pressure profile can also be generated in the shock tube by reducing the length of the HPC and/or using lighter gas (like helium) in the HPC. In the case of blast wave, the pressure profile is characterized by an abrupt pressure rise at the shock front (peak overpressure), followed by exponential decay to the atmospheric pressure levels.

Shock tube used in the present study has a HPC and LPC volume of 0.0454 m^3 and 0.012 m^3 respectively, with an internal diameter of 50 mm. The shock tube device is designed to operate in shock wave mode, with a wide range of shock strengths. In the current study, conventional metal diaphragm is replaced by a fast opening pneumatic valve (ISTA, St. Petersburg, Russia) having an opening time in order of 5 ms or less. The valve produces well-defined repeatable shock waves at ambient pressure conditions (Britan et al., 2001). The sample mounting section is attached at the end of the LPC, followed by a void space chamber (VSC). Schematic diagram of the shock tube assembly is shown in Fig. 2. A digital pressure gauge is fixed at the HPC to record the fill pressure at the time of release of the valve. Shock wave of desired strength can be generated by varying the fill pressure in HPC. In order to measure the shock wave velocity and pressure, piezoelectric pressure transducers (PCB 112 A-Series) P_1 and P_2 are flush mounted at the tail end of the LPC and the transducers P_3 and P_4 are mounted in the VSC. The pressure signal data are stored using a DL750 Yokogawa scope recorder with a sampling rate of 500 kHz.

2.2. Materials used and sample preparation

In the present study, three different kinds of granular materials are used as the infill materials, namely coarse sand (CS), fine sand (FS) and glass beads (GB). The particle size of CS varies from 1.18 mm to 4.75 mm and the grain size of FS particle lies between 0.075 mm and 2.36 mm, both classified as poorly graded with symbol 'SP' as per Unified Soil Classification System. In order to evaluate the effect of shape and surface features of the infill material, glass beads are selected as the comparative infill material to the coarse sand. The soda lime glass beads are smooth surfaced and are spherical in shape with particle size of 3 mm and 4 mm (in proportion of 50:50). The properties of coarse sand (CS), fine sand (FS) and glass beads (GB) are listed in Table 1 and the grain size distribution of the three different infill materials is shown in Fig. 3.

Stainless steel wire mesh and/or geotextile layer are used as a protective facing formwork to support the infill granular materials. The wire mesh is plain steel rolled wire of 0.5 mm diameter with a square opening aperture grid of 2.5 × 2.5 mm. The geotextile fabric used in the study is a polypropylene woven geotextile of thickness 0.6 mm. Tensile strength of the geotextile and the wire mesh is tested in accordance with the test methods ASTM D4595 and ASTM D4964 respectively. The material properties of geotextile and wire mesh are listed in Table 2.

The barrier sample model is prepared using a cylindrical stainless steel sample holder with an internal diameter of 50 mm (equal to ID of the shock tube). The thickness (or length, L = 50 mm) of the sample is kept constant throughout the study. The sample holder is provided with grove along the rim of the upstream and downstream edges, which would fecilitate in binding the facing

Table 1
The properties of different infill materials used in the present study.

Parameter	Find sand (FS)	Coarse sand (CS)	Glass bead (GB)
d_{10} (mm)	0.26	1.8	2.9
d_{50} (mm)	0.7	2.75	3.5
C_u	3.07	1.67	1.2
C_c	0.96	1.15	0.94
e_{max}	0.97	0.88	0.76
e_{min}	0.53	0.55	0.58
RD (%)	52.4	53.2	54.7
Porosity	0.47	0.46	0.45
Images			

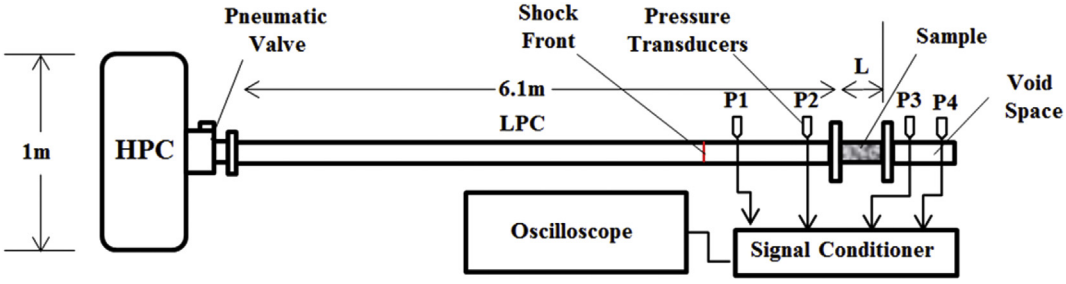

Fig. 2. Schematic diagram of the shock tube assembly.

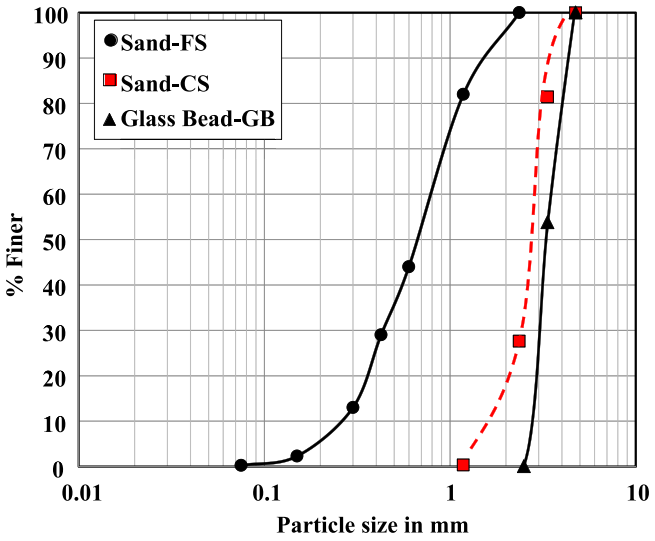

Fig. 3. Grain size distribution of different infill materials.

Table 2
The properties of geotextile and wire mesh.

Parameter	Geotextile	SS wire Mesh
Thickness, t (mm)	0.6	0.5
Mass per unit area, (g/m^2)	247	801
Tensile strength, kN/m	55	20

formwork. A preweighed quantity of the granular material is poured into the sample holder and the desired bulk density is achieved by controlled tamping. All test samples are carefully prepared to achieve a relative density of 53% (±1) which corresponds to bulk unit weight of 15.2 kN/m^3, 15.6 kN/m^3 and 15.8 kN/m^3 for CS, GB and FS respectively. The sample holder is then firmly held inside the slot provided in the VSC (Fig. 4a). The VSC along with the sample holder is inturn connected to the tail end of the LPC. This assembly ensures the sample is aligned along the axis of shock tube with a fixed end condition. Pressure transducers P_1 and P_2 are mounted on the upstream side, while P_3 and P_4 are mounted on the downstream side of the sample.

2.3. Experimental procedure

The experiments carried out in this study are broadly classified into six test cases (graphically described in Fig. 5). The primary aim of the experiments is to obtain the pressure signals on the upstream and downstream sides of the sample holder. Initial experiments are performed to understand the role of wire mesh and geotextile as a structural facing formwork. Without any granular infill, shock impact test is carried out on the wire mesh (test case-1). The purpose of test case-1 is to examine the influence of the wire mesh alone in attenuating the pressure levels of the incident shock wave. Further, test case-4 is performed to evaluate the effectiveness of the woven geotextile against shock impact loads. Further, several experiments of varying input shock strength are carried out to investigate the performance of coarse grain sand (CS) as the infill material with the wire mesh as the formwork medium (test case-2). Test case-3 is performed by replacing the coarse grain angular particle (CS) with a uniformly graded smooth glass beads (GB). The combined effect of the particle shape and surface characteristics (roughness) on the barrier is analyzed by comparing the test case-3 with that of test case-2. Finally, experiments are conducted by encapsulating the infill granular materials (CS and FS) in a geotextile lined wire mesh formwork (test case 5 and 6).

As mentioned in Section 2.1, experiments involved in the present study are designed to generate shock loading (with a flat-top plateau region). The strength of the shock wave is generally defined using incident shock Mach number and the corresponding pressure behind the incident shock front i.e., the peak incident pressure (overpressure). Mach number (M_s) is defined as ratio of the velocity of the shock wave in a given medium to the velocity of the sound in the same medium. A shock wave is a thin transitive area propagating at supersonic speed ($M_s > 1$) and it is characterized by an abrupt change in flow properties like pressure, density and temperature. The velocity of the incident shock wave (prior to the impact) in a shock tube is calculated by 'time of flight' method, measuring the time interval between the signals recorded by transducers P_1 and P_2.

All the experiments (test case 1 to 6) are carried out using nitrogen as the driving gas in the HPC, while LPC is kept at ambient atmospheric conditions. The pneumatic valve is released upon filling the required pressure in the HPC. A series of compression waves are generated in the LPC, which eventually coalesce to form a shock wave. A blank test case (without the test sample) is executed for different fill pressures in HPC. The shock tube is operated over a range of input shock strength with the incident shock Mach numbers (M_s) of 1.29, 1.43, 1.57 and 1.70 and the corresponding peak incident pressures (in bar) are 0.71, 1.12, 1.64 and 2.05. Fig. 6 compares the pressure data recorded by upstream pressure transducers P_1 for different shock intensities. A distinct plateau pressure region is observed at the end of the first jump, indicating a constant pressure zone travelling behind the incident shock front. Subsequently, the pressure behind the shock front increases upon reflection at the end wall. Similar pressure profiles can be observed later as transmitted wave in the downstream side of the test sample. The steady (plateau) pressure value is used for the calculation of the attenuation coefficient (K_a), given by expression:

$$K_a = \frac{Downstream\ Pressure\ behind\ Transmitted\ Wave}{Upstream\ Pressure\ behind\ Incident\ Shock\ Wave}$$

Further, the measurements of the incident pressure behind the shock front allow us to compare with the 'peak overpressure' of the free field blast wave and relate it to the detonation of a TNT charge at a specific standoff distance from the target (Kingery and Bulmash, 1984). For instance, a hemispherical explosive charge of 7 kg of TNT detonating at standoff distance of 5.82 m from the barrier, would generate an incident pressure of 1.12 bar and reflected pressure of 3.18 bar, these pressure ranges are comparable with the test condition with M_s equal to 1.43 (see Fig. 6).

3. Results and discussion

3.1. Attenuation of shock wave due to presence of steel wire mesh

The pressure data recorded from the test case-1 are shown in Fig. 7. The first jump seen in the signal of P_2 is the incident shock wave and the second jump corresponds to the reflected shock wave from the wire mesh. The first jump observed in P_4 signal is due to passage of the transmitted shock wave through the wire mesh and the second jump is due to the reflection from the end wall of the void space chamber. The incident and transmitted Mach number for the wire mesh case is found to be 1.43 and 1.41 respectively. It is observed that the transmitted wave through the mesh is travelling at supersonic velocity. However, depending on the type of barrier, the transmitted wave gets attenuated to a very weak shock wave or

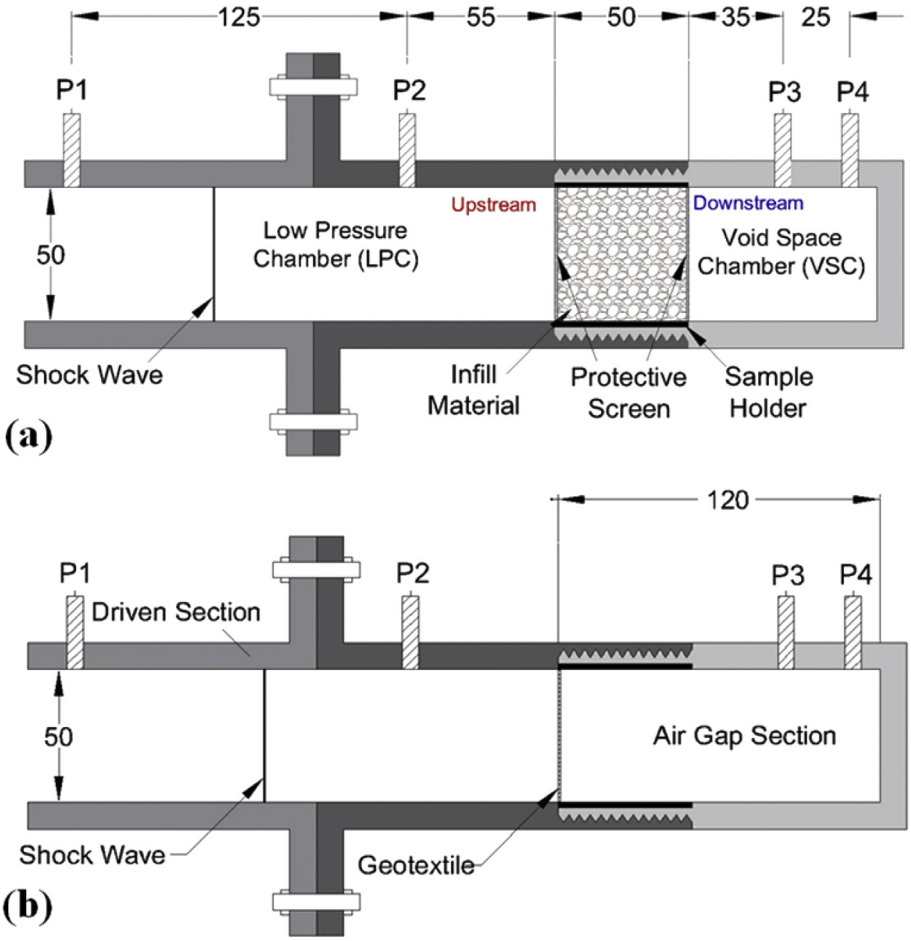

Fig. 4. a–b. Expanded view of the sample mounting section applicable to (a) Test case 2, 3, 5 and 6 with appropriate infill material and (b) Test case 4. (*All dimensions are in mm*).

TEST CASE	CASE: 1	CASE: 2	CASE: 3
U/S D/S Sample holder	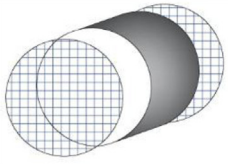	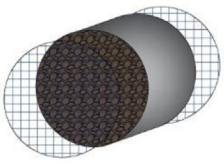	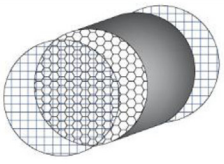
Upstream Face	SS MESH	SS MESH	SS MESH
Downstream Face	SS MESH	SS MESH	SS MESH
Infill Material	BLANK	SAND - CS	GLASS BEAD

TEST CASE	CASE: 4	CASE: 5	CASE: 6
U/S D/S Sample holder	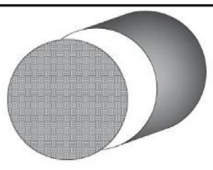	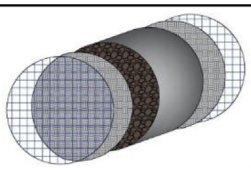	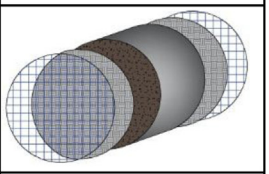
Upstream Face	GEOTEXTILE	SS Mesh + Geotextile	SS Mesh + Geotextile
Downstream Face	-	SS Mesh + Geotextile	SS Mesh + Geotextile
Infill Material	BLANK	SAND - CS	SAND - FS

Fig. 5. The configuration of the six test cases carried out in the present study.

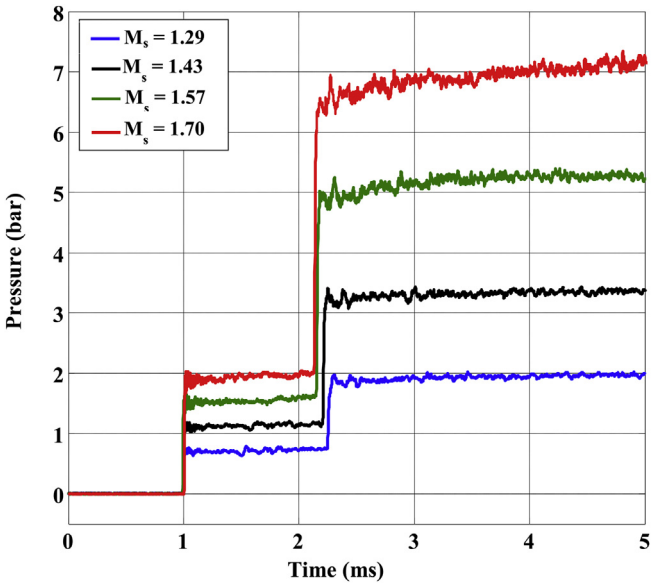

Fig. 6. The input pressure signals recorded by pressure transducer P_1 of the shock tube.

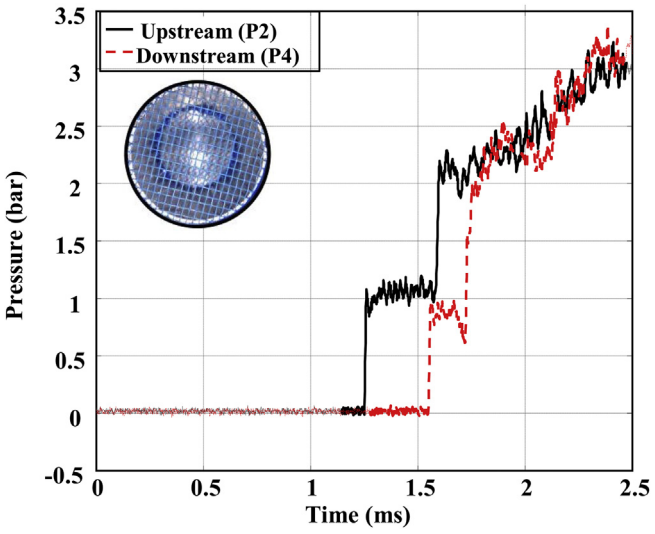

Fig. 7. Pressure-time history for test case-1 (wire mesh).

a subsonic ($M_s < 1$) compression wave (Ben-Dor et al., 1997; Mazor et al., 1994). Notably, there is a slight drop in pressure between the incident shock and the transmitted shock due to the presence of the mesh. The shock attenuation co-efficient value is found to be 0.84.

3.2. Attenuation of shock wave through granular medium

The pressure traces obtained during a shock ($M_S = 1.43$) barrier (CS) interaction is shown in Fig. 8 (test case −2). As expected, the downstream pressure has a different trend when compared to pressure signal of test case 1 (Fig. 7). In order to have better representation, the pressure profiles from all the transducers P_1–P_4 are plotted in space-time domain (popularly known as x-t diagram), which demonstrates shock propagation phenomena inside the shock tube. The y-axis represents the LPC of the shock tube; the sensors and the sample locations are appropriately scaled and identified on the ordinate axis. Each division on the y-axis

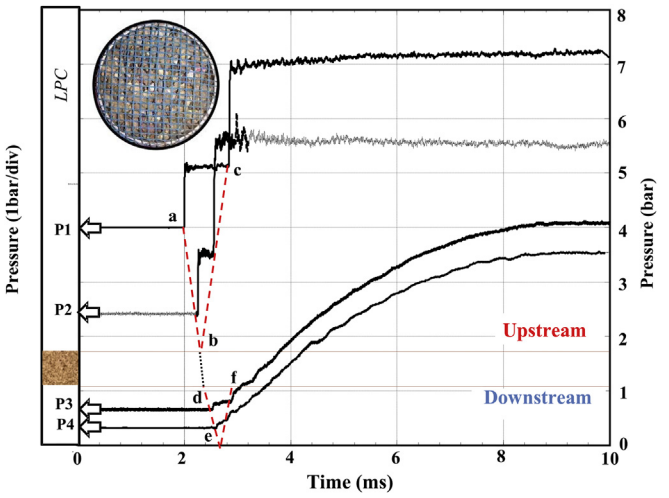

Fig. 8. Pressure histories recorded at upstream and downstream side for test case-2 (coarse sand).

corresponds to a pressure of 1 bar (equal to 10^5 N/m^2) and the x-axis corresponds to the time domain in millisecond (ms).

The construction lines (dashed line in red) shown in Fig. 8 represents the trajectories of the shock waves. The line ab is drawn by connecting the foot of the first jump observed in the pressure profiles of P_1 and P_2, which corresponds to the passage of the incident shock wave. Upon impinging on the sample, a part of the incident shock wave (ab) gets reflected as reflected shock wave (bc), while the rest of it passes through the granular sand media as a transmitted wave (bd). This transmitted wave emerges out on the downstream side as a shock wave/compression wave (de). After reaching the end of the shock tube wall (VSC), the transmitted wave further gets reflected into a reflected transmitted wave (ef). After the second pressure jump on the downstream end (P_3 and P_4), no further noticeable pressure jumps are observed. However, pressure continues to rise asymptotically (through gas filtration process) to reach an equilibrium condition (P_e) with the upstream pressure levels. In the present case, the transmitted wave is a weak shock wave with Mach number 1. In the x-t diagram, the angle of incident ray (angle between the incident trajectory path on the sample surface and the line perpendicular to the sample surface at the intersectional point of the incident trajectory) and the transmitted ray is found to be 9° and 18° respectively. Increase in the angle of the transmitted trajectories indicates the delay in the arrival time of the shock in the downstream end. With the attenuation coefficient value of 0.169, the coarse sand (CS) together with wire mesh has assisted in bringing down the pressure levels in the downstream side to about 17% of the incident pressure levels.

In order to consider the effect of particle shape and surface roughness, additional experiments are performed using spherical particles (glass beads-GB). The comparison of pressure profiles recorded at P_3, with CS and GB as infill material for incident shock M_s of 1.43 (test case-3) is shown in Fig. 9. It is observed that the initial pressure rise and plateau region of the GB matches exactly with that of CS. Henceforth, not much of a change is reflected on the K_a value. However, at the rise of the second jump, the pressure signal of GB exhibits slightly higher pressure and gradually isolates itself from CS. Upon impact load, the granular media is expected to undergo particle breakage and/or tend to relocate with enhanced interlocking. It is reasonable to believe that the shock induced pressure has assisted in the compaction of sand particles to a much denser state. The spherical particles have a lower degree of particle-particle interlock when compared to the angular particles. This

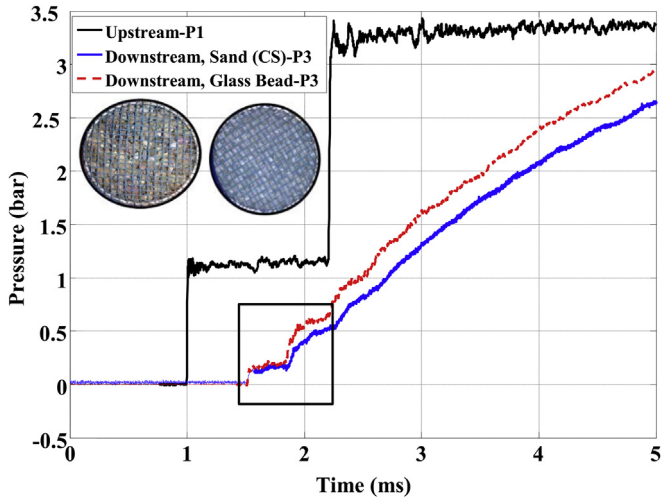

Fig. 9. Pressure-time history for test case-2 (coarse sand) and test case-3 (glass bead).

effect is characteristically observed at the rise of the second jump shown in Fig. 9. The compacted sand (CS) medium impedes the gas flow significantly compared to GB, thereby decreasing the downstream pressure and eventually increasing the time to attain the equilibrium pressure (P_e).

The mitigating capability of the infill materials (CS and GB) for varying incident Mach numbers is shown in Fig. 10. The attenuation co-efficient value is found to decrease with the increase in the incident Mach number. The glass bead and coarse sand (CS) have the same effects on K_a even at higher shock strength. It is also evident that the particle shape and roughness have minimum effect on the attenuation behavior. However, the infill material with angular shape seems to favor particle interlocking and is considered to be more efficient in delaying the filtration process. Normally, the delicate targets located on the downstream side of the barrier are expected to withstand a gradual buildup of pressure than a sudden increase in pressure. Hence, the longer the time taken to attain equilibrium pressure, the better is the functional behavior of the barrier system.

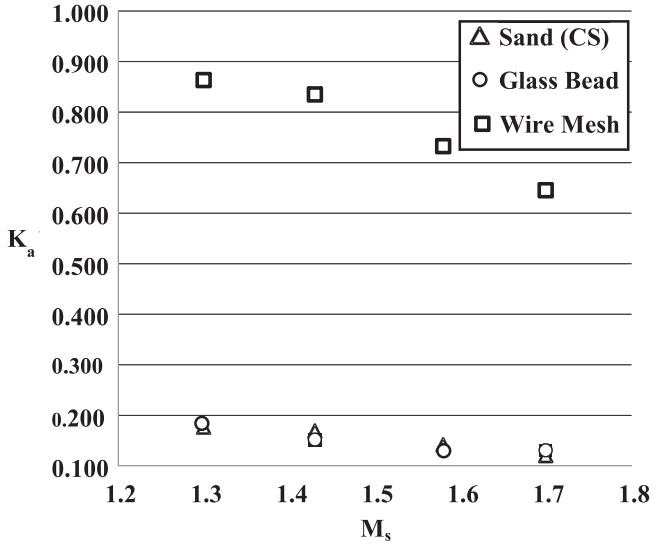

Fig. 10. A plot of attenuation coefficient versus the incident shock wave Mach numbers.

3.3. Shock wave interaction with geotextile layer

The geotextile is cut into 75 mm diameter samples and are placed on the upstream face of the sample holder. The geotextile is held tight in position by wrapping a strong adhesive tape around the rim of the sample holder. The sample holder is placed at the end of the LPC such that geotextile is facing the incoming shock wave, as shown in Fig. 4b. Though the main interest of this section is to assess the geotextile survivability upon shock impact, the downstream pressure levels are also recorded over a larger air gap of 120 mm. The pressure profile recorded for the test case-4 with an incident shock, M_s of 1.43 is shown in Fig. 11. In the absence of any kind of obstacle (infill material), the transmitted wave travels further till the end wall. Multiple sharp peaks are observed at the downstream side of the geotextile (signal P_3 of Fig. 11). These peaks are due to the repeated reflections between the geotextile layer and the end wall. The amplitude of the transmitted shock wave becomes smaller with the increase in the number of the reflections. A transmitted wave with M_s of 1.17 is formed in the downstream side with an attenuation coefficient of 0.33.

Scanning electron microscope (SEM) micrograph images of the geotextile layers are captured before and after the impact of the shock wave, at magnification of 100× (Fig. 12a–b). Geotextile layers on exposure to shock wave with M_s of 1.29, have little or no effect on the strands. While slightly increasing the Mach number to 1.43, geotextile has undergone slight surface deformity. Because of the impact force and the high temperature of the shock wave (around 180 °C), the polypropylene strands of geotextile have melted to form globule like structures. Upon further increasing the shock strength to M_s equal to 1.57, the geotextile can no longer resist the impact force and thereby it ruptures (Fig. 12c). The tensile stress and the flexural rigidity of the geotextile have significant influence on the occurrence of the failure.

From the attenuation results, it is observed that geotextile by itself appears to be more efficient than the widely spaced wire mesh. However, because of the low tensile stress and flexural rigidity, geotextile alone cannot be considered a stable formwork. The permeable geotextile fabric together with wire mesh will act as reliable formwork structure for the infill sand particles. Since a fabric like geotextile is considered to be a part of the formwork, extreme care must be taken during the infill material compaction. The formwork should be held in position such that proper contact is ensured between the geotextile and infill materials. Moreover, if there exists any gap (between geotextile and infill material), the

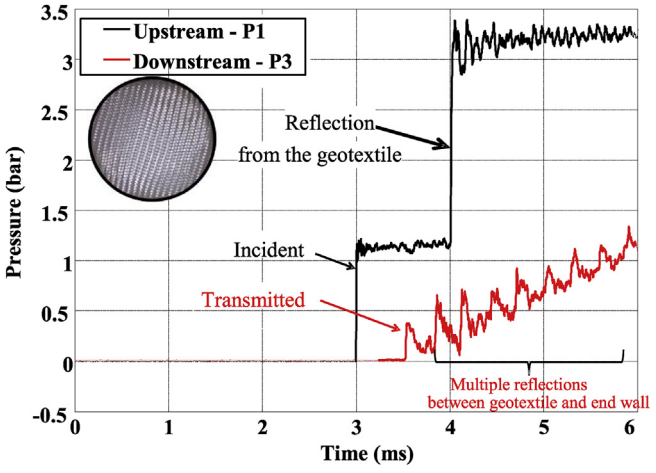

Fig. 11. Pressure-time history for test case-4.

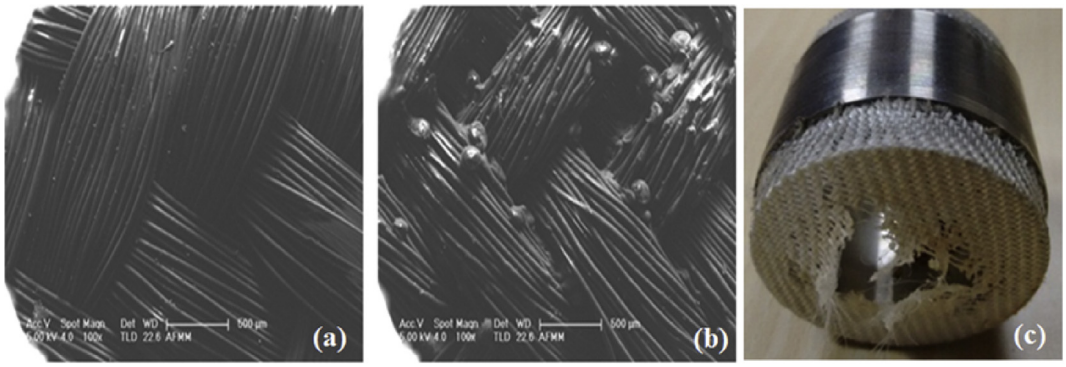

Fig. 12. a–c. SEM Images of geotextile layer for $M_s = 1.43$ (a) Before shock impact (b) After shock impact (c) Photograph of ruptured geotextile for $M_s = 1.57$.

pressure level adjacent to the geotextile is expected to amplify (as observed by Hattingh and Skews, 2001; Skews et al., 2010) and the encapsulated barriers will result in low structural stability.

3.4. Influence of geotextile layer on the sand barrier system

As mentioned previously (by Ben-Dor et al., 1997), shock wave impact on granular medium transmits a wave in the granular medium which is followed by two major processes: i) Pore volume compression, pore pressure increases and effective stress transfer takes place through particle-particle contact, ii) Gas filtration, where the entrained gas behind the shock wave passes through the pores of the granular medium overcoming the drag resistance.

The downstream pressure profiles for the test cases ($M_s = 1.43$) involving coarse sand barrier (CS), geotextile faced coarse sand barrier (G-CS) and geotextile faced fine sand barrier (G-FS), is summarized in Fig. 13. By close inspection of the pressure traces of G-CS, the plateau region of the transmitted wave (compression wave) is still visible. A delayed filtration process has resulted in a weak compression wave with lower pressure levels when compared to barrier system without geotextile facing. The strength of the transmitted wave further diminishes when the encapsulated barrier is filled with FS. It is evident from the pressure profiles of G-FS that there is a gradual rise in the pressure (without any jump or plateau region), which implies that steady-state gas filtration has taken place through the sand particles. The presence of geotextile layer on FS and CS has also decreased the slope of the quasi-steady pressure rise curve leading towards the equilibrium pressure (P_e).

The K_a value is plotted against a non-dimensional parameter, normalized barrier length (or thickness) L/d_{50} where L is the length of the sample and d_{50} is the average particle diameter (Table 1). The comparison of the experimental results ($M_s = 1.46$) of Britan et al. (2001) on glass particles of different sizes with the results obtained in present study ($M_s = 1.43$), is shown in Fig. 14. Though there is a slight variation in the M_s value, one can infer the results for comparison purpose. The K_a value for the glass beads compares well with that of Britan et al. (2001) value. Let us consider 0.5 mm glass bead infill of Britan et al. (2001), K_a value of 0.05 is reported for a sample of length, $L \approx 108$ mm. By using a geotextile facing on the barrier unit of length 50 mm and with a FS infill ($d_{50} = 0.7$ mm), the coefficients of attenuation are found to be much smaller ($K_a = 0.032$). For lower L/d_{50} ratio, the presence of geotextile has reduced the K_a value drastically to about 40%–50% to that of the unprotected barrier. The fact that geotextile aids in shock wave attenuation, implies that the barrier can further reduce the wall thickness.

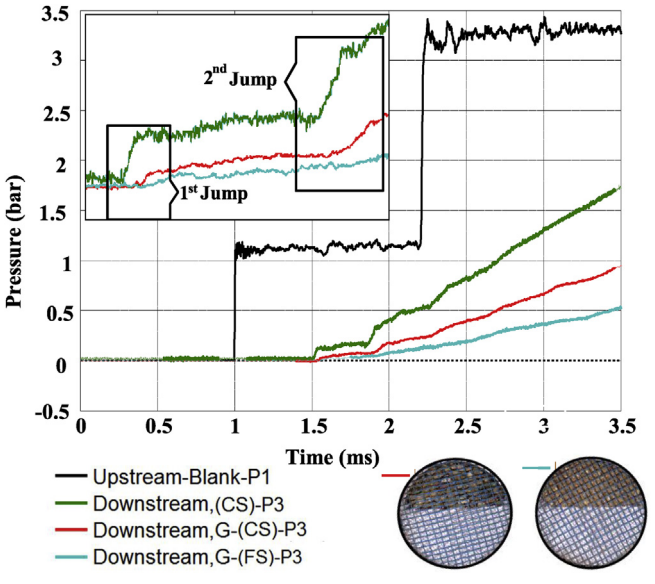

Fig. 13. Comparison of pressure signals from test case 2, 5 and 6. *Inset fig*: Magnifies the section between 1.5 and 2 ms.

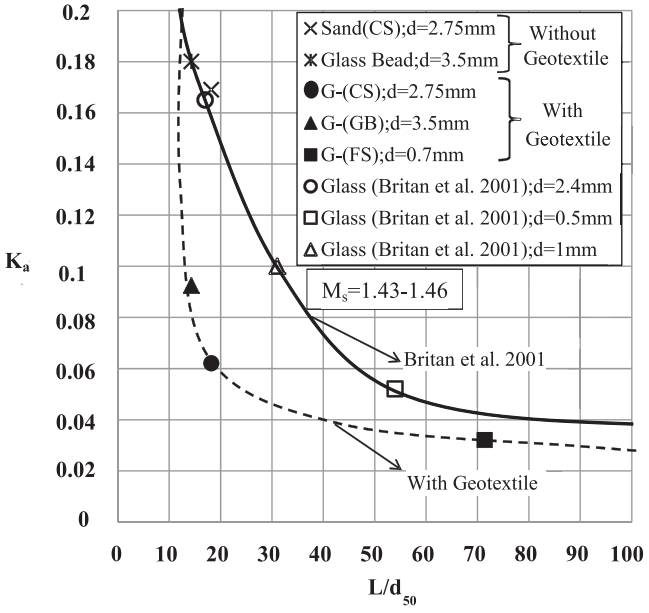

Fig. 14. Attenuation coefficient versus the normalized barrier length.

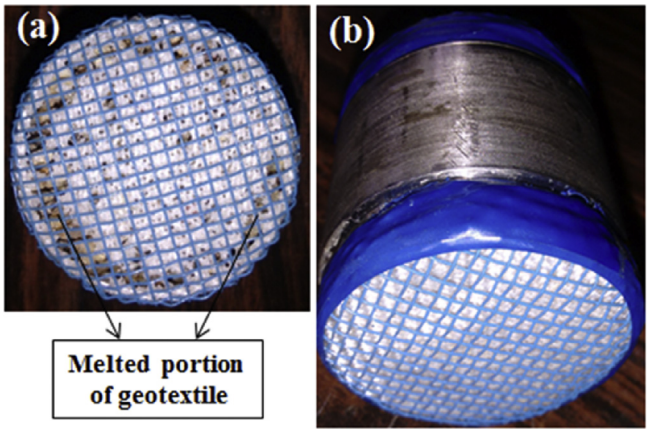

Fig. 15. a–b Picture of geotextile faced coarse sand barrier model after shock impact (a) Upstream side (b) Downstream side.

Furthermore, tests are carried out on the encapsulated barriers by increasing the strength of the shock wave (M_s > 1.53). It is observed that single layer of geotextile fabric on the upstream end could not withstand the high temperature and the pressure impact induced by the shock wave (See Fig. 15a). The sand particles are released out of the sample holder through the damaged portion of the geotextile, thereby decreasing the compaction of the infill sand. The wire mesh on the upstream end has also undergone minor damages at certain intersection joints. However, the geotextile and the wire mesh on the downstream end of the sample seem to be unaffected (See Fig. 15b). The geotextile layer on the barrier system has contributed significantly; it primarily serves as a confinement enclosure for the infill granular materials. Geotextile facing prevents the direct contact of the shock wave on the granular particles. The steel wire mesh provides structural stability, while geotextile acts as a shield against the shock wave impact and especially that of secondary fragments (such as debris, shrapnel, shattered glass, etc). Though geotextile is a permeable membrane, it impedes the gas flow to some extent. The flow impedance caused by the geotextile affects the gas filtration process and subsequently decreases the rate at which downstream pressure equilibrates.

In order to assess the stability of the system, series of experiments (M_s = 1.43) are carried out by mounting the accelerometer on the supporting formwork. From the experimental results, it is observed that the pressure level of the reflected shock against the upstream face of the barrier is always higher than the incident shock. Hence, it is important to ensure that the upstream supporting formwork of the barrier system can withstand the pressure generated by the reflected shock wave. The shock resistance of the barrier system is evaluated by measuring the displacement-time histories at critical points on the barrier systems. Two accelerometers are installed on the barrier system, one at the upstream face and the other at the downstream face of the formwork. The complete assembly and the positions of the accelerometer are shown in Fig. 16 a–c. The accelerometers used are piezo crystal type-resistive transducers manufactured by PCB Electronics (M353B17). The accelerometers are mounted using an adapter, which is then firmly affixed on the wire mesh and the geotextile layer. Accelerometer (A_{us}) on the upstream end is embedded in the infill material, while the accelerometer (A_{ds}) is mounted on the rear end of the barrier system. The presence of the miniature accelerometer (7 mm diameter x 12.4 mm length, with a mass of about 1.7 g) inside the infill material and the wires extending out of the sample is assumed to have minimal effect. The displacement response of the system is indirectly obtained by double integration of the recorded acceleration signal.

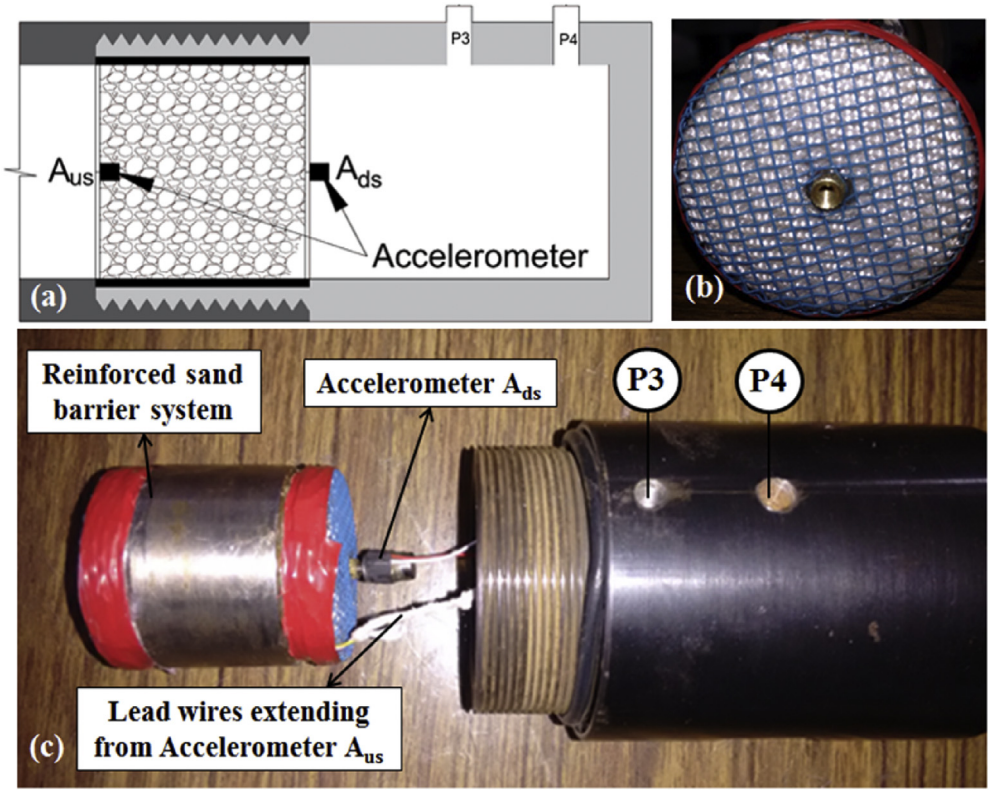

Fig. 16. a-c (a) Schematic cross section showing the location of accelerometer (b) Adapter mounted on the downstream section (c) Overview of the assembly with sample holder.

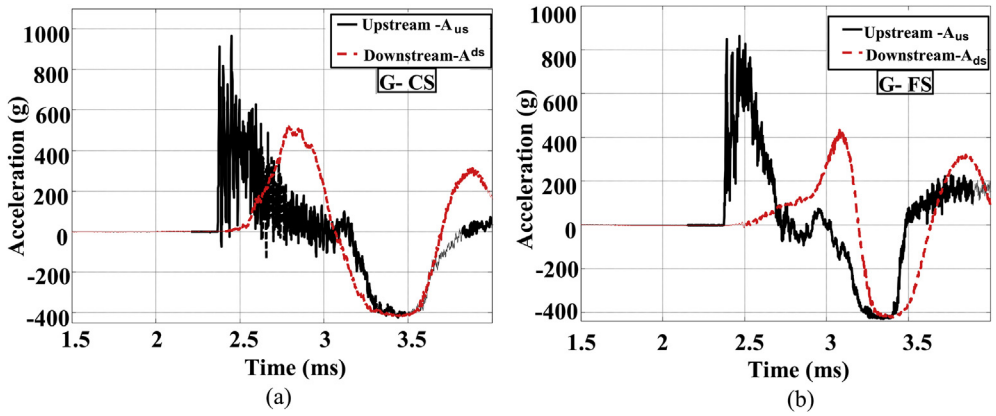

Fig. 17. a–b. The acceleration-time history for the test case involving geotextile encapsulated barrier system with infill material: (a) coarse sand and (b) fine sand.

The acceleration responses are captured at sampling rate of 500 kHz for each of the test case over a period of 4 ms. The acceleration time histories of test case-5 (G-CS) and test case-6 (G-FS) are shown in Fig. 17a and b respectively. The peak acceleration value and the positive response of the upstream formwork are found to be similar in both the cases. Certainly, under this situation, the type of infill granular medium has little effect on the upstream formwork. However, the downstream peak acceleration response is found to be higher for coarse sand compared to fine sand infill.

The displacement time histories calculated from the acceleration response for CS infill is shown in Fig. 18a. As predicted, the deformation on the upstream end is observed to be larger than the downstream value. The confined sand together with the upstream formwork offers most of the resistance to the impinging shock. The deformation on the downstream end is mainly due to the effective stress transfer through the particles. In order to ascertain that, displacement responses are evaluated from the results of fine sand infill (G-FS). There is a substantial decrease in the displacement on the downstream side when compared to the coarse sand (see Fig. 18b). This observation is explained with the help of an illustrative diagram shown in Fig. 19a–c. When a shock wave impinges on unprotected granular media, contact forces develop between individual particles and the induced stress primarily gets transferred through particle-particle contact (Terzaghi et al., 1996). When compared to the spherical particle, the contact area between the particles is higher for an angular shaped particle. Increase in the

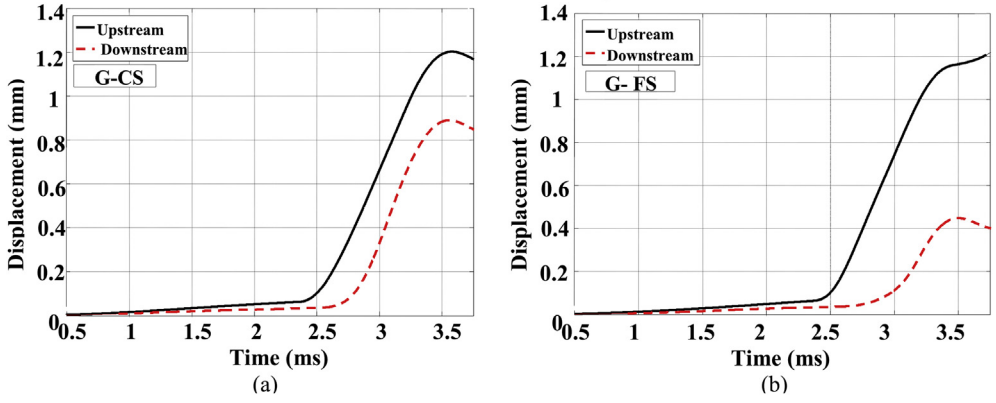

Fig. 18. a–b. The displacement-time history for test case involving geotextile encapsulated barrier system with infill material: (a) coarse sand and (b) fine sand.

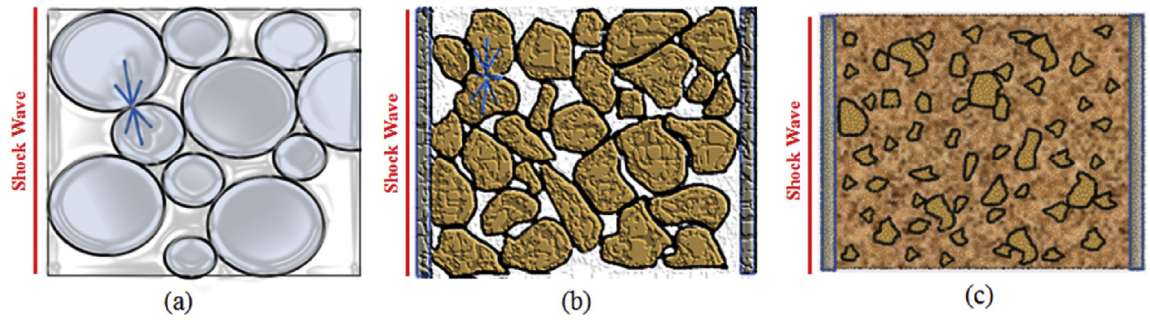

Fig. 19. a–c. Illustration of particle arrangement in different barrier system: (a) Glass bead barrier (GB) (b) Geotextile faced coarse sand barrier (G-CS) (c) Geotextile faced fine sand barrier (G-FS).

contact area effectively decreases the magnitude of the effective stress. In the case of the fine sand, the small grain particles are suspended within the matrix of fines and the interacting area with the adjacent particles becomes large. Consequently, the stress induced from the fine sand to the downstream formwork is lower.

4. Conclusions

The present work has demonstrated the effectiveness of geotextile encapsulated sand barriers in attenuating the shock waves. The interaction between shock wave and rigid barrier is investigated using a shock tube. The shock tube experiments are operated at Mach numbers from 1.29 to 1.7, the geotextile-lined barrier system performance is analyzed using coarse and fine sand as infill materials. The shock wave attenuation co-efficient is derived from the pressure-time history recorded on the upstream and downstream end of the sample.

The attenuation coefficient (K_a) is dependent on the average particle size (d_{50}) and thickness of the barrier. As the mean particle size of the sand decreases, there is a notable reduction in the K_a value, while there is no significant effect of particle shape and surface features on the attenuation co-efficient. However, angular shaped sand particles have prominent role in delaying the time taken to reach equilibrium pressure (P_e). The primary function of the geotextile is to provide a formwork along with the wire mesh for the infill granular materials. In addition to this, geotextile prevents the direct contact between the shock wave and the sand particles, thereby reducing the magnitude of the stress transfer. The presence of the geotextile has significantly reduced the gas pressure exiting the encapsulated barrier and also decreased the rate at which downstream pressure equilibrate (P_e). The lower the K_a value and longer the time taken to reach P_e, the better is the performance of the barrier system. On the basis of the results of this study, a geotextile encapsulated barrier system can be designed with appropriate infill material for an optimized thickness, thereby offering an efficient protection system against shock loads. Such an impact protection system can be successfully implemented in both military and commercial applications.

A functional limitation of the geotextile encapsulated barrier system is that they operate at low-moderate shock strengths. The woven-geotextile could not withstand the high temperature and the pressure imparted by the shock wave. Also, the present study has emphasized mainly, the issues associated with interaction of air shock and the barriers, and has not considered the impact caused due to secondary effects (such as debris, shrapnel, chemical and UV degradation, etc.). Nevertheless, these barrier systems can still be operated at such extreme conditions by reinforcing the formwork with wire mesh of high tensile strength and using multiple layers of geotextile (or using a heavy duty geotextile). Further studies are necessary in order to investigate the infill particle size, moisture effects, type and quality of geotextile and the thickness of the barrier units against strong air shock and secondary fragments.

References

Afzali-Nejad, A., Lashkari, A., Shourijeh, P.T., Influence of particle shape on the shear strength and dilation of sand-woven geotextile interfaces, *Geotext. Geomembr.* 45 (1), 54–66.

Athanasopoulos, G.A., 1993. Effect of particle size on the mechanical behavior of sand-geotextile composites. Geotext. Geomembr. 12 (3), 255–273.

Bathurst, R.J., Vlachopoulos, N., Walters, D.L., Burgess, P.G., Allen, T.M., 2006. The influence of facing stiffness on the performance of two geosynthetic reinforced soil retaining walls. Can. Geotech. J. 43 (12), 1225–1237.

Ben-Dor, G., Britan, A., Elperin, T., Igra, O., Jiang, J.P., 1997. Experimental investigation of the interaction between weak shock waves and granular layers. Exp. Fluids 22, 432–443.

Britan, A., Ben-Dor, G., Igra, O., Shapiro, H., 2001. Shock waves attenuation by granular filters. Int. J. Multiph. Flow 27, 617–634.

Britan, A., Ben-Dor, G., Shapiro, H., 2007. The contribution of shock tubes to simplified analysis of gas filtration through granular media. J. Fluid Mech. 586, 147–176.

Britan, A., Jiang, J.P., Igra, O., Elperin, T., Ben-Dor, G., 1997. Gas filtration during the impact on weak shock waves on granular layers. Int. J. Multiph. Flow 23 (3), 473–491.

Costa, C.M.L., Zornberg, J.G., Bueno, B.D., Costa, Y.D.J., 2016. Centrifuge evaluation of the time-dependent behavior of geotextile-reinforced soil walls. Geotext. Geomembr. 44, 188–200.

Engebretsen, T., Bakken, J., Hansen, E.W.M., Lysberg, I., 1996. Shock waves and gas flow through granular materials. In: Proceeding Workshop Explosion Effects in Granular Materials. Norway, Oslo, pp. 111–131.

Guler, E., Selek, O., 2014. Reduced-scale shaking table tests on geosynthetic-reinforced soil walls with modular facing. J. Geotech. Geoenvironmental Eng. 140 (6), 04014015.

Hattingh, T.S., Skews, B.W., 2001. Experimental investigation of interaction of shock waves with textiles. Shock Waves 11, 115–123.

Heffernan, P.J., Moyle, C.C., Wight, R.G., Scherbatiuk, K.D., 2006. The effectiveness of textile barriers to attenuate blast wave ingress into buildings. In: Proceedings. 1st International Structural Specialty Conference. Canadian Society for Civil Engineering, Calagary, Canada. DM-029, 1–8.

HESCO Bastion concertainers®, 2010. Citing Online Sources. http://www.hesco.com/.

Hong, Y.S., Wu, C.S., Yu, Y.S., 2016. Model tests on geotextile-encased granular columns under 1-g and undrained conditions. Geotext. Geomembr. 44 (1), 13–27.

Jiang, Y., Han, J., Parsons, R., Brennan, J., 2016. Field instrumentation and evaluation of modular-block MSE walls with secondary geogrid layers. J. Geotech. Geoenvironmental Eng. 142 (12), 05016002.

Kingery, C.N., Bulmash, G., 1984. Airblast Parameters from TNT Spherical Air Burst and Hemispherical Surface Burst. Technical Report ARBRL-TR-0255. Ballistics Research Laboratory, Aberdeen Proving Ground, Maryland, USA. http://www.un.org/disarmament/un-saferguard/kingery-bulmash/.

Koerner, R.M., Soong, T.Y., 2001. Geosynthetic reinforced segmental retaining walls. Geotext. Geomembr. 19 (6), 359–386.

Koerner, R.M., Wilson-Fahmy, R.F., Narejo, D., 1996. Puncture protection of geomembranes. Part III Ex. Geosynth. Int. 3 (5), 655–675.

Lee, K.M., Manjunath, V.R., 2000. Soil geotextile interface friction by direct shear tests. Can. Geotech. J. 37 (1), 238–252.

Ling, H.I., Leshchinsky, D., Tatsuoka, F., 2003. Reinforced Soil Engineering: Advances in Research and Practice. Marcel Dekker Inc., New York, pp. 359–389.

Liu, S.H., Gao, J.J., Wang, Y.Q., Weng, L.P., 2014. Experimental study on vibration reduction by using soilbags. Geotext. Geomembr. 42 (1), 52–62.

Lv, H., Wang, Z., Li, J., Experimental study of planar shock wave interactions with dense packed sand wall, *Int. J. Multiph. Flow* 89, 255–265, (in press)

Mazor, G., Ben-Dor, G., Igra, O., Sorek, S., Takayama, K., 1994. Shock wave interaction with cellular materials. Part: I analytical investigation and governing equations. Shock Waves 3, 159–165.

Narejo, D., Koerner, R.M., Wilson-Fahmy, R.F., 1996. Puncture protection of geomembranes. Part II Exp. Geosynth. Int. 3 (5), 629–653.

Ng, C., Chew, S., Karunaratne, G., Tan, S., Loh, S., 2000. Flexible and Rigid Faced Mechanical Stabilized Earth Walls Subject to Blasting. In: Advances in Transportation and Geoenvironmental Systems Using Geosynthetics. ASCE, Geo-Denver, pp. 332–336.

Palmeira, E.M., Tatto, J., 2015. Behaviour of geotextile filters in armoured slopes subjected to the action of waves. Geotext. Geomembr. 43 (1), 46–55.

Pieri, I.R., 1998. Using Reinforced Earth Walls for Blast Mitigation. M. E Thesis. University of Florida.

Portelinha, F.H.M., Zornberg, J.G., Pimentel, V., 2014. Field performance of retaining walls reinforced with woven and nonwoven geotextiles. Geosynth. Int. 21 (4), 270–284.

Rose, T.A., Smith, P.D., Mays, G.C., 1998. Protection of structures against airburst using barriers of limited robustness. Proc. Inst. Civ. Eng. Struct. Build. 128 (2), 167–176.

Sapko, M.J., Hieb, M.R., Weiss, E.S., Zipf, R.K., Harteis, S.P., Britt, J.R., 2009. Passive mine blast attenuators constructed of rock rubble for protecting ventilation seals. In: SME (Society for Mining, Metallurgy & Exploration Inc.) Annual Meeting and Exhibit and CMA's 111th National Western Mining Conference Proceedings.

Scherbatiuk, K., Rattanawangcharoen, N., 2008. Experimental testing and numerical modeling of soil-filled concertainer walls. Eng. Struct. 30 (12), 3545–3554.

Skews, B.W., Bugarin, S., Sawicka, E., 2010. Surface pressure effects from shock wave impact on inclined and curved clothing. Int. J. Impact Eng. 37 (3), 231–241.

Smith, P.D., 2010. Blast walls for structural protection against high explosive threats: a review. Int. J. Prot. Struct. 1 (1), 67–84.

Terzaghi, K., Peck, R.B., Mesri, G., 1996. Soil Mechanics in Engineering Practice, third ed. Wiley-Inter science Publication, New York, pp. 83–84.

Tognon, A.R., Rowe, R.K., Moore, I.D., 2000. Geomembrane strain observed in large scale testing of protection layers. J. Geotech. Geoenvironmental Eng. 126 (12), 1194–1208.

Van-der Grinten, J.G.M., Van Dongen, M.E.H., Van-der Kogel, H., 1985. A shock-tube technique for studying pore-pressure propagation in a dry and water-saturated porous medium. J. Appl. Phys. 58, 2937–2942.

Vangla, P., Latha, G.M., 2016. Effect of particle size of sand and surface asperities of reinforcement on their interface shear behavior. Geotext. Geomembr. 44,

254–268.
Wu, C.S., Hong, Y.S., 2009. Laboratory tests on geosynthetic encapsulated sand columns. Geotext. Geomembr. 27 (2), 107–120.
Yogendrakumar, M., Bathurst, R.J., 1992. Numerical simulation of reinforced soil structures during blast loads. Transp. Res. Rec. 1336, 1–8.
Zhiwei, H., 2009. Geosynthetics Structures Subject to Blast Load. Ph.D Thesis. National University of Singapore.

Nomenclature

LPC: Low Pressure Chamber
HPC: High Pressure Chamber
VSC: Void Space Chamber
ID: Internal Diameter
M_s: Mach number
L: Length or thickness of an the barrier model
d_{50}: Diameter for which 50% in weight of the soil particles have diameter smaller than that value
C_u: Soil coefficient of uniformity
C_c: Soil coefficient of curvature
$e_{max/min}$: Maximum or minimum void ratio
P_e: Equilibrium pressure
K_a: Coefficient of attenuation